Eur. Phys. J. D **41**, 475–483 (2007)
DOI: 10.1140/epjd/e2006-00245-5

THE EUROPEAN PHYSICAL JOURNAL D

Application of R-matrix method to electron-H_2S collisions in the low energy range

M. Gupta[a] and K.L. Baluja

Department of Physics and Astrophysics, University of Delhi, Delhi 110007, India

Received 24 August 2006 / Received in final form 13 October 2006
Published online 15 November 2006 –

Abstract. Electron-H_2S collision process is studied using the R-matrix method. Nine low-lying states of H_2S molecule are considered in the R-matrix formalism to obtain elastic integral, differential, momentum transfer and excitation cross sections for this scattering system. We have represented our target states using configuration interaction (CI) wavefunctions. We obtained adequate representation of vertical spectrum of the target states included in the scattering calculations. The cross sections are compared with the experiment and other theoretical results. We have obtained good agreement for elastic and momentum transfer cross sections with experiment for entire energy range considered. The differential cross sections are in excellent agreement with experiment in the range 3–15 eV. A prominent feature of this calculation is the detection of a shape resonance in $^2B_2$ symmetry which decays via dissociative electron attachment (DEA). Born correction is applied for the elastic and dipole allowed transition to account for higher partial waves excluded in the R-matrix calculation. The electron energy range is 0.025–15 eV.

PACS. 34.80.Bm Elastic scattering of electrons by atoms and molecules – 34.80.Gs Molecular excitation and ionization by electron impact

1 Introduction

Hydrogen sulphide, H_2S, is also called rotten egg gas. It is classified as a toxic chemical and in high concentration can be fatal. Large abundance of H_2S have been observed in the Orion Plateau [1]. The clouds of H_2S are present in the central star in the "Rotten Egg" nebula and are found in the extragalactic sources. The doubly deutrated H_2S has been detected by Vastel et al. [2]. Since the dipole moment of H_2S in its ground state at its equilibrium geometry is relatively large (0.98D), the electron scattering cross sections are expected to be large. The presence of a polar molecule in a gas even as a small impurity may effect the electrical conductivity of the gas.

Theoretically, ab initio work in the spectra of H_2S has been mainly concerned with the vertical spectrum at the ground-state equilibrium geometry of H_2S [3–10]. Three-dimensional ab initio calculations for the potential surfaces of the two lowest electronic states with $^1A''$ symmetry which map $^1B_1$ and $^1A_2$ electronic symmetries in C_{2v} point group have been presented [11]. The vertical energies of 36 excited states, arising from excitations from $2b_1$ and $5a_1$ molecular orbital have also been obtained [12] using SCF-Xα-SW calculations. Vast majority of the excited states are Rydberg states except those involving $6a_1$ and $3b_2$ excited orbitals.

Experimental data on excited states is also availabe from absorption spectra [13,14] and electron impact study [15]. Experimental vertical excitation values are also available [16–18]. Ionization potential for the ground state of H_2S has been measured by optical spectroscopy [16], by photoionization [19], by photoelectron spectroscopy [20], by binary $(e, 2e)$ electron impact [21] and via penning ionization electron spectrometry [22].

There exist several calculations of cross sections for electron-impact on H_2S. The first calculation [23] used a parametrized model to treat exchange and polarization forces. Various types of cross sections were reported [24,25] for the low-energy electron scattering by H_2S. In these calculations, the static potential was derived from molecular ground state near Hartree-Fock functions, the exchange term was treated in the free electron gas Hara-type approximation and the polarization effects were modelled by a parameter-free polarization potential. An ab initio optical potential has been used in the complex-Kohn variational method [26] for electron-H_2S elastic scattering for electron impact energy range 1–30 eV. The Schwinger variational iterative method [27] has also been used at the static-exchange (SE) level for the calculation of elastic differential, integral and momentum transfer cross-sections which covered the energy range 2–50 eV. At the SE level, Schwinger multichannel method [28,29] with pseudo potentials have been used to calculate these cross sections for energy up to 30 eV.

[a] e-mail: monika123_in@yahoo.co.in

A considerable number of cross section measurements have been done for electron-H_2S scattering. Absolute elastic differential cross sections (DCS) in vibrational stretching and bending mode have been measured by Rohr [30,31] for energies upto 10 eV. He found a broad shape resonance at 2.3 eV. In addition, absolute total cross sections have been reported using electron cyclotron resonance technique [32] and linear transmission method [33]. Relative elastic DCS have also been measured [34]. Absolute DCS for vibrationally elastic electron scattering using a crossed electronic-molecular beam apparatus have been measured [35] at incident energies from 1–30 eV and scattering angles between 20° and 130°. Information on low-lying anionic H_2S state is available from dissociative attachment results [36–40] and from electron transmission experiment [41].

In the present work, the electron-molecule scattering dynamics is treated in the R-matrix formalism [42,43]. The R-matrix code has already been used in a series of calculations, more recently being on H_2CO [44], O_3 [45] and SO_2 [46]. The calculation of rotationally elastic and inelastic DCS is carried out by using the program POLY-DCS [47]. The K-matrix elements required by this program are calculated in a 9-state R-matrix approach where each state is represented by a CI configuration.

2 R-matrix method

The R-matrix method [48,49] is based on the idea that the scattering problem is split into two separate spatial regions, an inner region and an outer region. The inner region is chosen in such a way that the charge density of the target is negligible at the boundary of the inner region. It is defined in the present case by a sphere of radius $15a_0$ centered at the H_2S centre of mass. In the inner region, the scattering electron lies within the molecular charge cloud and the exchange and correlation effects are strong. In the inner region, the wavefunction is written using the CI expression:

$$\Psi_k^{N+1} = A\sum_{ij}\phi_i^N(X_1,\ldots,X_N)\xi_j(X_{N+1})a_{ijk} + \sum_m \chi_m(X_1,\ldots,X_N,X_{N+1})b_{mk} \quad (1)$$

where, A is an anti-symmetrization operator, X_N is the spatial and spin coordinate of the Nth electron, ϕ_i^N represents the ith state of the N-electron target, ξ_j is a continuum orbital spin-coupled with the target states. The continuum functions do not vanish on the boundary of the inner region. The sum in the second term of equation (1) represents short-range polarization effects. To obtain reliable results, it is important to maintain a balance between the N-electron target representation, ϕ_i^N, and the $(N+1)$ electron scattering wavefunction. The choice of appropriate χ_m is crucial in this [50]. The coefficients a_{ijk} and b_{mk} are variational parameters which can be determind by solving an eigenvalue problem relevant to the inner region, where all the relevant integrals are evaluated for the spatial range 0–$15a_0$ by employing the standard bound state quantum chemistry methods. In practice, all the integrals are evaluated in the entire configuration space of the scattering system, the tail contribution outside the R-matrix sphere is subtracted.

In the first term of equation (1), the first summation is over the number of target electronic states included in the calculation and the second summation is over the number of continuum orbitals linked to each target state. The double summation in the first term of equation (1) generates 'target+continuum' configurations. The summation in the second term of equation (1) runs over configurations χ_m, where all electrons are placed in target occupied and virtual molecular orbitals. These are described as the L^2 configurations and are important for relaxing the orthogonality between the target and continuum orbitals. Gaussian-type orbitals (GTOs) are used to represent the bound and the continuum electrons. The main advantage of GTOs is that the multicentred integrals can be evaluated in a closed form. We have used the GTO continuum basis functions [51] in which these functions were fitted to Bessel functions for the case of a neutral molecule.

In the outer region, when the scattering electron is at a large distance from the center of mass of the target, the probability of swapping its identity with any of the target electron is negligible and so are the exchange and correlation effects. The interacting potentials are direct and are multi-polar in character. We include only the dipolar and quadrupolar potentials of the long-range character. The outer region is essentially a potential-field region, and we can use single center expansion of the scattering system analogous to equation (1) by dropping the antisymmetrization operator and also dropping the second summation involving correlation effects. This leads to a set of coupled differential equations, and the solution functions are propagated outward [52] until the effect of multipolar forces is negligible. These solutions are then matched with the appropriate standing wave boundary conditions yielding K-matrix, eigenphase sums and the cross sections.

3 Results and discussion

3.1 Target and scattering model

We used the double zeta plus polarization (DZP) Gaussian basis set (12,8,1)/(6,4,1) for S [53] and (5,2,2)/(3,2,2) for H [54] for our calculations on H_2S. We have not used a large basis set with diffuse functions as it extends outside the R-matrix box. H_2S is a bent molecule with $^1A_1$ symmetry ground state whose point group C_{2v} is of order four. We have employed the H_2S experimental equilibrium geometry [21,55] where S-H distance is taken to be 1.335 Å and the H-S-H angle is 92.11°. H_2S is formed by bonding each of the two unpaired 1s orbitals of hydrogen with the unpaired 3p orbital of sulphur. The Hartree-Fock electronic configuration for the ground state is $1a_1^2\ 2a_1^2\ 1b_2^2\ 3a_1^2\ 1b_1^2\ 4a_1^2\ 2b_2^2\ 5a_1^2\ 2b_1^2$. The molecular orbitals are generated by performing a self-consistent field (SCF) calculation at the experimental equilibrium geometry of the ground state

Table 1. Dominant configuration, transition moment of each transition from the ground state in au, and the vertical excitation energies in eV for the target states of H_2S.

State	Configuration	Transition moment	Vertical excitation energy (eV)				
			This work	Roberage et al. [12]		Shih et al. [4]	Expt.
				Theo.	Expt.	Theo.	
X^1A_1	$5a_1^2 2b_1^2 2b_2^2$	0.385	–	–	–	–	
1^3A_2	$\ldots 2b_1^{-1} 3b_2$	0.000	6.70	5.88	≤ 6.3	6.17	
1^1A_2	$\ldots 2b_1^{-1} 3b_2$	0.000	7.08	6.30	–	6.80	4.60-7.50 [16] 7.4 [18]
1^3B_1	$\ldots 2b_1^{-1} 6a_1$	0.000	7.21	5.75	–	5.91	
1^1B_1	$\ldots 2b_1^{-1} 6a_1$	0.215	7.50	6.13	5.0–7.4	6.22	6.33 [16]
1^3B_2	$\ldots 5a_1^{-1} 3b_2$	0.000	9.24	8.14	–	8.46	
2^3B_1	$\ldots 2b_1^{-1} 7a_1$	0.000	9.40	7.69	8.18	7.75	
2^3A_2	$\ldots 2b_1^{-1} 4b_2$	0.000	9.97	7.62	–	7.67	
2^1A_2	$\ldots 2b_1^{-1} 4b_2$	0.000	10.07	7.64	–	7.69	

of the H_2S molecule. These SCF wavefunctions of the target are calculated from standard contracted basis sets and the SCF energy is found to be –398.678 au. In the present work, CI wavefunctions are used to represent all the target states. We divided our calculation into 10 core electrons fully occupied in the 5 molecular orbitals and 8 valence electrons which are free to occupy $4a_1$, $5a_1$, $6a_1$, $7a_1$, $2b_1$, $2b_2$, $3b_2$ and $4b_2$ molecular orbitals. The vertical excitation energies for the excited states so formed lie in the range 6.70–10.07 eV.

In Table 1 we list the dominant configurations, the transition moments and the vertical excitation energies for the target states obtained in the present work and compared these with other theoretical and experimental work. The first entry (0.385 au) in the transition moment column refers to dipole moment of the ground state of the molecule. We have fair agreement with the experimental and other theoretical results. To provide additional information on the charge distribution in H_2S molecule, we have also calculated the dipole and quadrupole moments of H_2S at its equilibrium geometry. Our SCF model yields a dipole moment of 0.406 au. The value is higher than the experimental value of 0.382 au [33]. The corresponding value obtained by our CI model is 0.385 au, which is in excellent agreement with the experimental value. The absolute values of quadrupole components Q_{20} and Q_{22} for the ground state in our CI model are 0.673 au and 1.260 au respectively. Since there are no measured values for quadrupole moments of the ground state of H_2S, we have compared our computed values with the available theoretical values [56]. The value of our Q_{20} component is in good agreement with the SCF value 0.674 au, and is slightly less than the value 0.796 au, evaluated at the level of many perturbation (MP2) theory in which triple-zeta plus polarization basis functions are employed.

The origin is kept at the centre of mass for all the calculations. Our scattering calculations included the nine target states given in Table 1, in the close-coupling expansion of the system. Calculations were performed for doublet A_1, A_2, B_1 and B_2 scattering symmetries. The continuum orbitals were represented by Gaussians centered at the molecule centre of gravity to represent Bessel functions within the finite region of the R-matrix sphere [51]. These orbitals depend parametrically on the R-matrix spherical radius and the range of incident electron-impact energies, and are independent of the target molecule. Our calculations were performed for continuum orbitals up to g-partial wave. These continuum orbitals were orthogonalized to the target orbitals based on a mixture of Schmidt and Löwdin symmetric orthogonalization methods, and those continuum orbitals with an overlap of less than 2×10^{-7} were removed [42]. It is important to preserve the balance between the amount of correlation included in the target states and in the scattering calculation. This is achieved by allowing 9 electrons (8 valence electrons +1 scattering electron) to move freely among $4a_1$, $5a_1$, $6a_1$, $7a_1$, $2b_1$, $2b_2$, $3b_2$ and $4b_2$ molecular orbitals.

3.2 Differential cross sections

Our calculations are carried out in the fixed nuclei (FN) framework which is valid since the collision time is much smaller than the characteristic times of nuclear motion. However, the evaluation of elastic DCS for polar molecules in the FN approximation leads to divergence in these cross sections in the forward direction. This divergence can be avoided by introducing rotational motion of the molecule. The elastic DCS is then obtained by summing up rotationally resolved elastic and inelastic cross sections which are extracted from the K-matrix elements calculated in the 9-state R-matrix method. The evaluation of DCS is a stringent test for any scattering theory employed. These cross sections play an important role in several areas of investigation like atmospheric physics, plasma physics, radiation biology etc. The DCS for a general polyatomic molecule can be explained as:

$$\frac{d\sigma}{d\Omega} = \sum_L A_L P_L(\cos\theta) \qquad (2)$$

Table 2. Energies of rotational levels of the electron-H_2S scattering system.

J	τ	Energy (meV)	J	τ	Energy (meV)
0	0	0.0	4	–4	14.358
1	–1	1.719		–3	14.358
	0	1.881		–2	18.510
	1	2.404		–1	18.538
2	–2	4.765		0	21.236
	–1	4.798		1	21.654
	0	6.366		2	21.732
	1	6.852		3	24.322
	2	7.245		4	24.463
3	–3	8.969	5	–5	20.940
	–2	8.973		–4	20.940
	–1	11.858		–3	26.305
	0	12.011		–2	26.309
	1	13.360		–1	30.379
	2	14.327		0	30.486
	3	14.580		1	32.894
				2	33.748
				3	34.533
				4	36.854
				5	36.925

where P_L is a Legendre function. The A_L coefficient have already been discussed in detail [57]. For a polar molecule this expansion over L converges slowly. To circumvent this problem, we use the closure formula

$$\frac{d\sigma}{d\Omega} = \frac{d\sigma^B}{d\Omega} + \sum_L \left(A_L - A_L^B\right) P_L(\cos\theta). \tag{3}$$

The superscript B denotes that the relevant quantity is calculated in the Born-approximation with an electron-point dipole interaction. The convergence of the series is now rapid since the contribution from the higher partial waves to the DCS is dominated by the electron-dipole interaction. The quantity $d\sigma^B/d\Omega$ for any initial rotor state $|j\tau\rangle$ is given by the sum over all final rotor states $|j'\tau'\rangle$

$$\frac{d\sigma^B}{d\Omega} = \sum_{j'\tau'} \frac{d\sigma^B(j\tau \to j'\tau')}{d\Omega}. \tag{4}$$

The expressions of state-to-state rotationally inelastic DCS, $d\sigma^B(j\tau \to j'\tau')/d\Omega$ for a spherical top, a symmetric top and an asymmetric top molecules are already been given [47]. The rotational eigenfunctions and energy levels of H_2S, which is an asymmetric top molecule are calculated by the program ASYMTOP [24] for all values of J up to 5. The eigen values are reported in Table 2. We used the calculated rotational constants for H_2S at its equilibrium geometry, which are 10.349153 cm^{-1}, 9.043974 cm^{-1} and 4.826322 cm^{-1} to calculate these rotational energy levels. Since there is no vacancy in the ground state of molecule H_2S, the scattering electron can occupy one of the low-lying virtual orbitals $6a_1$, $3b_2$, $7a_1$ and $4b_2$ which have SCF orbital energies equal to 3.51 eV, 4.06 eV, 5.39 eV and 5.99 eV respectively at the equilibrium geometry of the H_2S molecule. We have calculated rotationally summed

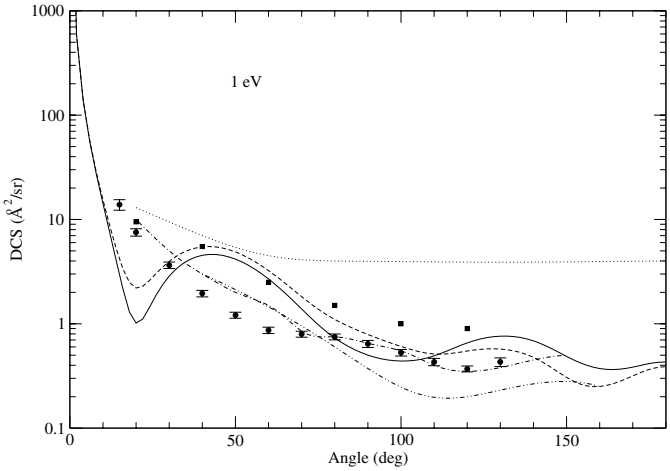

Fig. 1. DCS at 1 eV: dashed curve, present work (SE); full solid curve, present work (CI); experiment: solid circle, Gulley et al. [35]; solid square, Rohr [31]; theory: dotted curve, Gianturco [25]; double-dot dashed curve, Jain and Thompson [24]; dot-dashed curve, Lengsfield [26].

DCS for elastic scattering of electrons from H_2S molecule at incident electron energies 1, 2, 3, 5, 10 and 15 eV in the angular range from 0° to 180°. The sum is from the initial rotational level $J = 0$ to final rotational levels $J' = 0$, 1, 2, 3, 4, 5. In this we included all the nine states in the close coupling expansion. The K-matrix elements from a particular scattering R-matrix calculation form input to the computational code [47] which yields the DCS, elastic and momentum transfer cross sections.

In Figure 1, we have shown DCS calculated by the R-matrix method at SE and the 9-state scattering models at 1 eV. We have compared these with the available experimental [31,35] and other theoretical [24–26] values. Our 9-state curve lies lower than our SE curve due to the loss of flux in a multistate calculation. At such low energy, all the theoretical results by different methods are at variance with each other. Only the complex-Kohn calculation [26] seem to agree with the experimental data [35]. Almost a similar situation exists at 2 eV as shown in Figure 2. As the energy increases from 3 eV and above, we find good agreement between our results and the experimental results [35] as shown in Figures 3 to 7. This agreement improves as the energy increases. We also notice a general agreement among all the theoretical values shown. In Figure 5, we have presented the $(0 \to 0, 1, 2, 3, 4, 5)$ rotational transition cross-sections at an incident energy of 10 eV. These cross sections have been summed over the final pseudo quantum number τ'. The rotational elastic scattering $(0 \to 0)$ has the dominant contribution, whereas the dipole component $(0 \to 1)$ has the characteristic forward peak. The undulations in $(0 \to 1)$ cross sections have also been noticed in the other Schwinger variational calculation [27]. The quadrupolar component $(0 \to 2)$ exhibit an almost flat curve which is in conformity with born results. As J' increases to 5, the cross section contribution becomes negligible thus ensuring that our DCS have converged with respect to J values. At 15 eV, there are

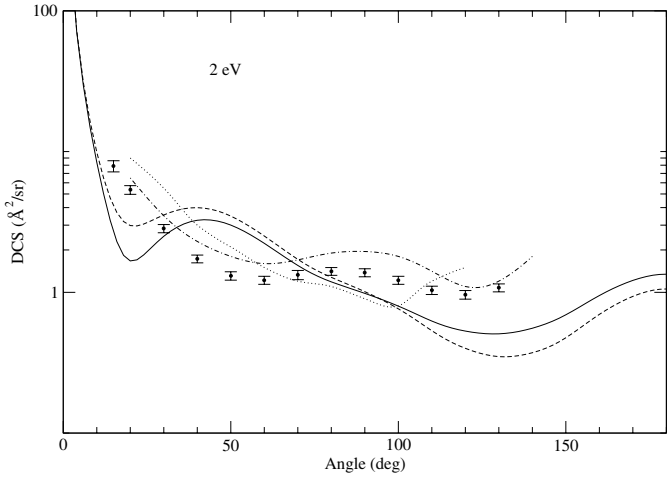

Fig. 2. DCS at 2 eV: dashed curve, present work (SE); full solid curve, present work (CI); experiment: solid circle, Gulley et al. [35]; theory: dotted curve, Gianturco [25]; dot-dashed curve, Lengsfield [26].

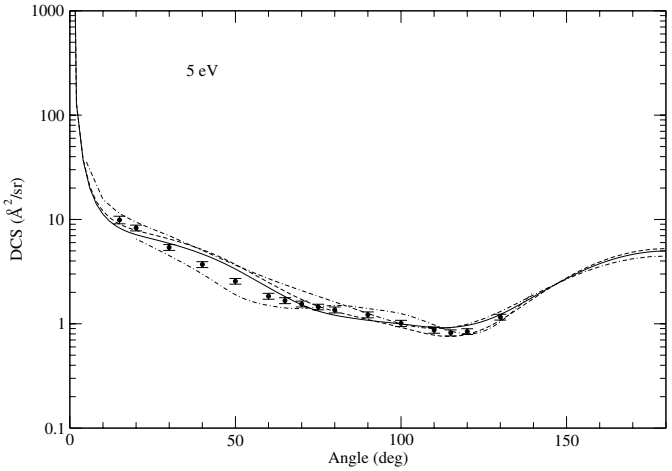

Fig. 4. DCS at 5 eV: dashed curve, present work (SE); full solid curve, present work (CI); experiment: solid circle, Gulley et al. [35]; theory: double-dash dotted curve, Natalense et al. [29]; dot-dashed curve, Lengsfield [26].

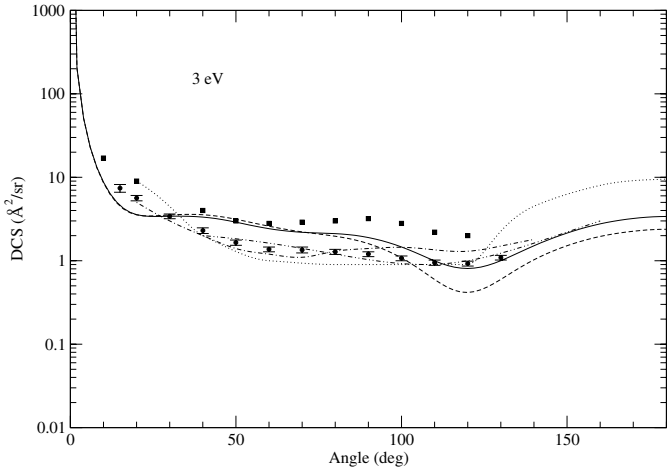

Fig. 3. DCS at 3 eV: dashed curve, present work (SE); full solid curve, present work (CI); experiment: solid circle, Gulley et al. [35]; solid square, Rohr [31]; theory: dotted curve, Gianturco [25]; double-dot dashed curve, Jain and Thompson [24]; dot-dashed curve, Lengsfield [26].

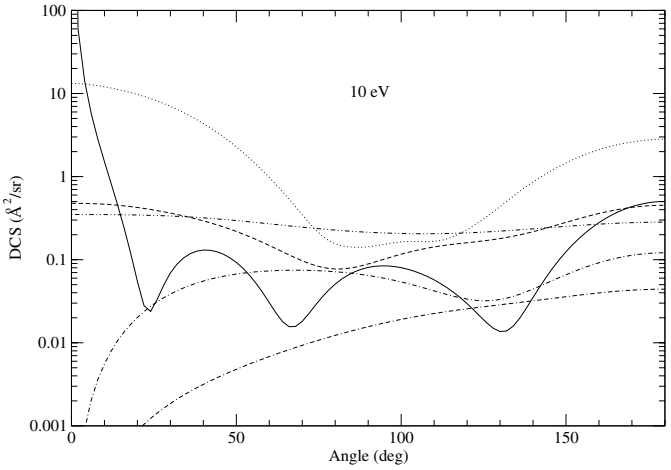

Fig. 5. DCS for various rotational excitations at 10 eV: dotted curve, $J = 0 \rightarrow J' = 0$; full curve, $J = 0 \rightarrow J' = 1$; dashed curve, $J = 0 \rightarrow J' = 2$; dot-dashed curve, $J = 0 \rightarrow J' = 3$; double-dot dashed curve, $J = 0 \rightarrow J' = 4$; double-dashed dot curve, $J = 0 \rightarrow J' = 5$.

two minima in DCS, which occur near 70° and 135° indicating the dominance of d-wave scattering caused by the heavier atom sulphur. As energy increases from 1 eV to 10 eV, we notice that backward scattering increases and reaches maximum at around 4 eV which is close to the resonance position, and then decreases. This is typical behaviour of DCS near a resonance position in the case of polar molecules.

3.3 Elastic integral cross sections

In Figure 8 we have shown integrated elastic cross-sections of our 9-state R-matrix results. We also performed an SE calculation in which we used only the ground state of the molecule described by the SCF calculation, in the close coupling expansion of the scattering system. As energy approaches zero, we notice the dominance of dipole scattering contribution. The peak at threshold is due to A_1 symmetry, in which the incoming electron occupies the first vacant orbital, $6a_1$, that predominantly involves s-wave scattering. A prominent feature of the elastic cross section curve is the appearance of $^2B_2$ shape resonance. The peak of the resonance lies at 4.74 eV with a width of 2.24 eV in the SE model. This resonance is also connected with a sudden increase of about π radian in the eigenphase sum in a multichannel calculation. By fitting the eigenphase sum to the Breit-Wigner profile the position and width of this resonance is determined. These parameters agree well with the corresponding values of 5 eV and 3 eV as calculated by Gianturco [25] in single centre expansion at the same level of SE treatment. In our

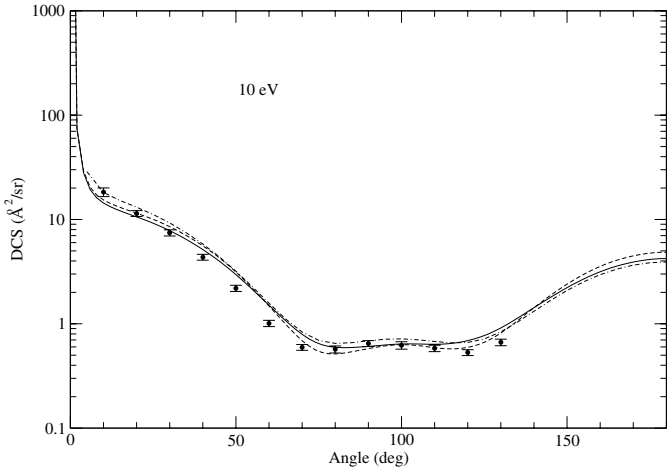

Fig. 6. DCS at 10 eV: dashed curve, present work (SE); full solid curve, present work (CI); experiment: solid circle, Gulley et al. [35]; theory: double-dash dotted curve, Natalense et al. [29].

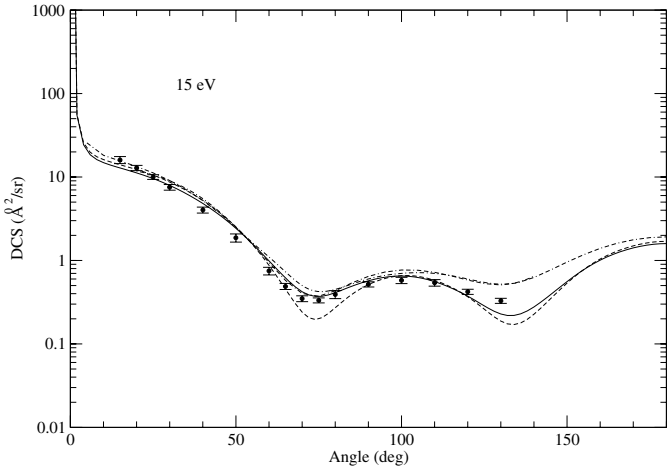

Fig. 7. DCS at 15 eV: dashed curve, present work (SE); full solid curve, present work (CI); experiment: solid circle, Gulley et al. [35]; theory: double-dash dotted curve, Natalense et al. [29]; dot-dashed curve, Lengsfield [26].

CI calculation, this resonance shifts to 3.86 eV with the corresponding width of 1.92 eV. This is to be compared with the values calculated by Jain and Thompson [24] who found resonance in $^2B_2$ symmetry at 2.22 eV with the corresponding width of 1.31 eV. The effect of the resonance in the elastic cross section appears as a hump. In a shape resonance phenomenon, the incident electron with a non-zero angular momentum, is trapped by the centrifugal barrier to form a temporary negative molecular ion H_2S^- that decays via quantum mechanical tunneling. The elastic cross section calculated in a 9-state R-matrix method lies lower than SE curve of R-matrix calculation for almost the entire energy range. The inclusion of correlation in the target states and the loss of flux in the additional scattering channels provided in a multistate calculation lowers the cross sections with respect to calculation performed at SE level. Our cross sections have been compared with the experimental [35] and other theoretical results [24,25,27,28] and a good agreement is found in general. Due to the presence of a long-range dipole interaction, the elastic cross section is formally divergent in the fixed-nuclei approximation due to a singularity in the differential cross section in the forward direction. To obtain converged cross sections, the effect of rotation must be included along with a very large number of partial waves. The effect of partial waves higher than $l = 4$ partial wave was included using Born correction which requires expressions for the partial as well as full Born cross sections. These expressions have been taken from the work of Chu and Dalgarno [60]. For applying the Born correction we have used the experimental value 0.382 au for the dipole moment of H_2S at its equilibrium geometry. It is worth mentioning that the elastic cross section for H_2S are higher than H_2O which has similar electronic configuration and geometrical structure. The results for DCS's for electron collisions with water give better agreement than DCS's results for H_2S. This may be due to the enlarged active space of H_2S that involve $3s$ and $3p$ atomic orbitals of S, that require extra correlation effects to properly describe the charge cloud of molecular orbitals of H_2S in its ground and excited states.

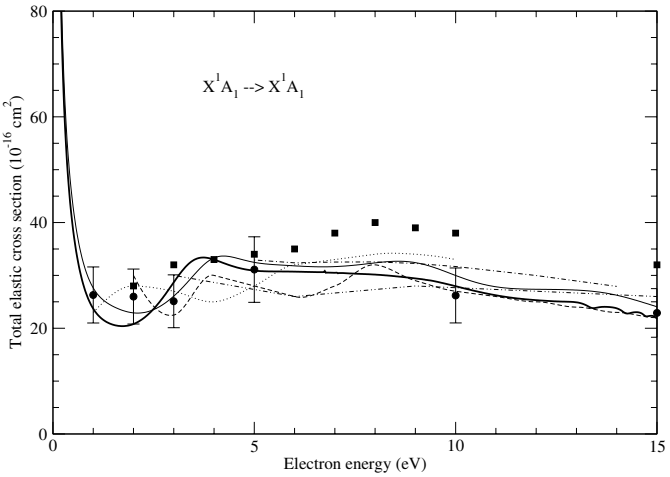

Fig. 8. Total elastic cross sections (9-state R-matrix for electron impact on H_2S: light solid curve, present work (SE); dark solid curve, present work (CI); experiment: solid circle, Gulley et al. [35]; solid square, Szmytkowski et al. [33]; theory: dotted curve, Jain and Thompson [24]; dashed curve, Machado et al. [27]; dot-dashed curve, Varella et al. [28]; double-dot dashed curve, Gianturco [25].

3.4 Momentum transfer cross section

A further test of the quality of our DCS is shown in Figure 9, where we have shown momentum transfer cross section (MTCS), which is defined as:

$$\sigma_m = 2\pi \int \frac{d\sigma}{d\Omega}(1 - \cos\theta)d\theta. \quad (5)$$

The MTCS indicates the importance of the backward scattering and is an important quantity that forms the input

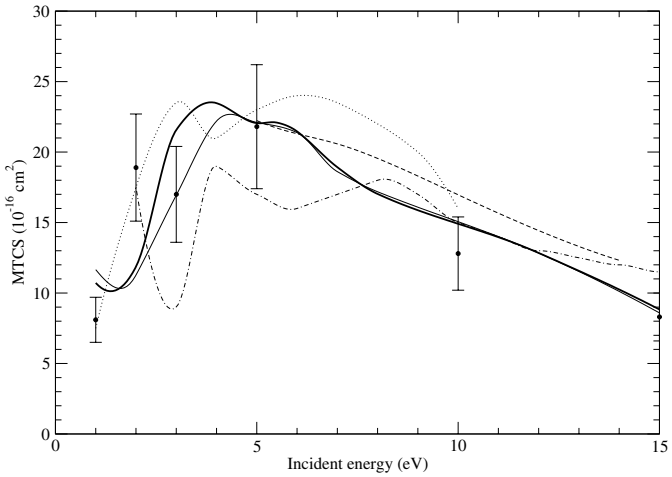

Fig. 9. The momentum transfer cross section for electron scattering by H_2S: light solid curve, present work (SE); dark solid curve, present work (CI); experiment: solid circle, Gulley et al. [35]; theory: dotted curve, Jain and Thompson [24]; dashed curve, Varella et al. [28]; dot-dashed curve, Machado et al. [27].

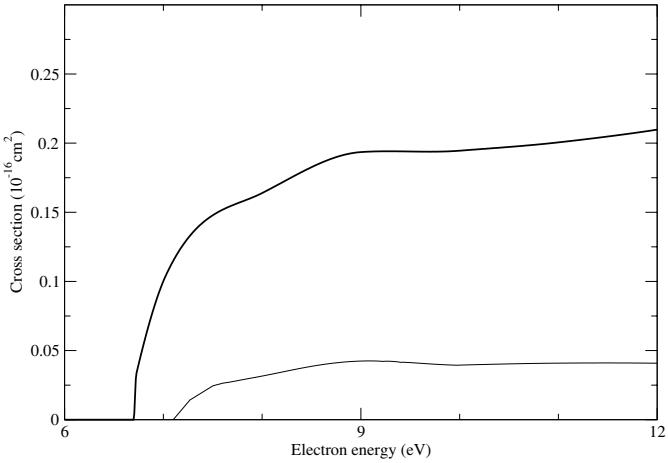

Fig. 10. Electron impact R-matrix excitation cross sections: dark solid curve, $X^1A_1 \rightarrow 1^3A_2$ symmetry; light solid curve, $X^1A_1 \rightarrow 1^1A_2$ symmetry.

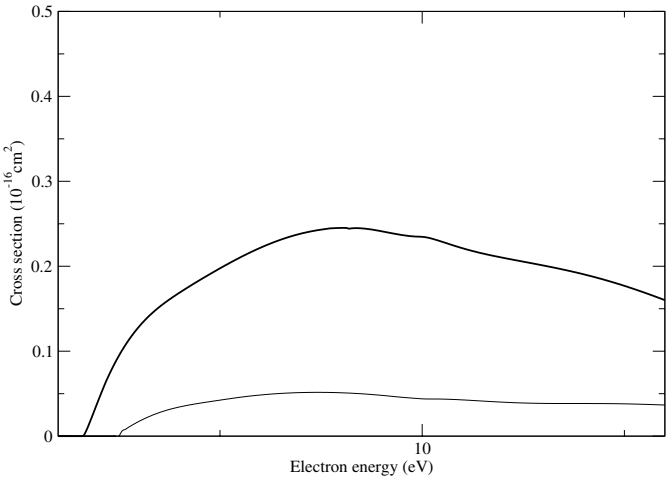

Fig. 11. Electron impact R-matrix excitation cross sections: dark solid curve, $X^1A_1 \rightarrow 1^3B_1$ symmetry; light solid curve, $X^1A_1 \rightarrow 1^1B_1$ symmetry.

to solve the Boltzmann equation for the calculation of electron distribution function of swarm of electrons drifting through a molecular gas. In contrast to the divergent behaviour of DCS in the forward direction, the MTCS does not diverge due to the multiplicative factor $(1-\cos\theta)$. Figure 9 shows our MTCS obtained in both SE and 9-state R-matrix approach and are compared with the experiment [35] and other available theory [24,27,28]. The peak at 3.86 eV shows the presence of $^2B_2$ resonance as already explained in Section 3.3. Beyond 5 eV, the curve is parallel to the curve of Varella et al. [28] but is consistently lower. The curve of Jain and Thompson [24] and Machado et al. [27] also depict peaks similar to the present work but at slightly different energies. Only our R-matrix results are in good agreement with experimental values.

3.5 Excitation cross section

Figures 10 and 11 present electron-impact excitation cross sections from the ground state to the first four excited states, in the 9-state R-matrix calculation. According to the optical dipole selection rules, the transitions to the triplet states are spin-forbidden, and the transitions to the states of A_2 symmetry are symmetry-forbidden. In the present spectrum only the transition to excited state $^1B_1$ is dipole allowed. The cross sections for these dipole allowed transitions have been Born corrected using the Born correction formula [60] except that the dipole moment is replaced by the transition moment of the concerned transition. In Figure 10, we have shown the excitation cross section for transitions $X^1A_1 \rightarrow 1^3A_2$ and $X^1A_1 \rightarrow 1^1A_2$. The cross sections for 1^3A_2 rises quickly from threshold and become nearly constant with a value of 0.2 Å^2. These cross sections are mostly composed of $^2B_2$ symmetry component. The cross section for 1^1A_2 symmetry is lower than its triplet counterpart due to its lower degeneracy which is 1/3 that of the triplet scattering symmetry. In the complete absence of exchange effects, this ratio becomes exact. In Figure 11, the cross sections for 1^3B_1 and 1^1B_1 symmetry are shown. Here also the 1^3B_1 curve lies above the 1^1B_1 state due to spin degeneracy effect. Here, the major contribution comes from $^2A_1$ symmetry. As the energy increases, due to the diminishing effect of exchange, the ratio of cross sections for triplet to singlet approaches the value corresponding to the ratio of their spin degeneracies.

4 Variation of resonance parameters with bond length

From the lowest R-matrix pole of $^2A_1$ symmetry, we notice that this state of H_2S^- is a virtual state with a very small excess energy of 0.14 eV with respect to the ground state of H_2S at its equilibrium position. Therefore, it does not show any resonance behaviour. To investgate the possible

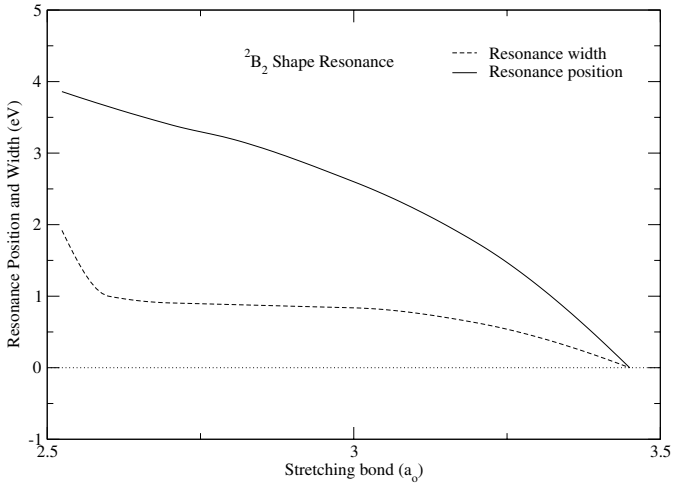

Fig. 12. Variation of $^2B_2$ shape resonance width and position with stretching bond (S-H) in C_s symmetry.

bound nature of $^2A_1$ scattering symmetry and the possible decay route of the detected shape resonance of $^2B_2$ symmetry, we carried out a series of R-matrix calculation in the 9-state model in which we stretched one bond of SH from its equilibrium value to about $3.5a_0$, while keeping other geometrical parameters of the molecule fixed. The calculations are performed in C_s point group, in which A′ symmetry correlates with A_1 and B_2 symmetries of C_{2v} point group and the other A″ symmetry of C_s correlates with the other two symmetries of C_{2v} point group. Variation of both the $^2A_1$ and $^2B_2$ scattering states is thus explored via A′ symmetry only. As the stretching increases, the $^2A_1$ scattering symmetry becomes a bound state near a distance of $3.45a_0$ and corresponds to the fragmentation channel:

$$H_2S^- \longrightarrow SH^-(^1\Sigma^+) + H(^2S).$$

This mechanism provides a method of producing SH negative ions. In Figure 12, we have shown the variation of resonance width and resonance position of $^2A'$ ($^2B_2$ in C_{2v}) shape resonance with stretching S-H bond. These resonance parameters decrease with increasing S-H bond length and approaches zero at $3.45a_0$. This implies that the shape resonance decays via DEA. This corresponds to the other two-body fragmentation channel:

$$H_2S^- \longrightarrow SH\ (^2\Pi) + H^-\ (^1S).$$

Since the electron affinity of SH is 2.314 eV, which is much higher than electron affinity of H (0.754 eV), we expect that as the energy of the incident electron increases from zero eV onwards, $SH^-(^1\Sigma^+)$ is formed first and then as energy increases further the other negative ion namely $H^-(^1S)$ is formed. This is confirmed by the appearance of DEA peaks of SH^- and H^- in the experiment [38]. We also made a calculation for the potential energy curve for H_2S with fragment products as H and SH. Our calculation yielded a value of 3.34 eV for the dissociation of H_2S into these products, which closely agree with the experimental value of 3.26 eV [61].

5 Conclusion

The elastic differential, integral, momentum transfer and excitation cross sections for electron impact on H_2S are calculated using the R-matrix method with an adequate target representation. For the low-lying excited states, we have good agreement between the vertical spectrum of these states with experiment. The dipole moment of the ground state is also in excellent agreement with the experimental results. Our calculation shows shape resonance in $^2B_2$ symmetry at the equilibrium geometry of H_2S molecule. This is in conformity with the other results obtained with a much larger basis functions, which included diffuse functions. For $^2B_2$ symmetry, the scattering electron temporarily occupies the $3b_2$ orbital, which is dissociated leaving the H^- ion via DEA. The elastic and momentum transfer cross sections are in good agreement with the experimental results. DCS in the range 5–15 eV, are also in excellent accord with the experiment. Excitation cross sections for low lying excited states have been presented for the first time.

References

1. Y.C. Minh, W.M. Irvine, D. McGonagle, L.M. Ziurys, Astrophysical J. **360**, 136 (1990)
2. C. Vastel, T.G. Phillips, C. Ceccarelli, J. Pearson, The Astrophysical J. **593**, L97 (2003)
3. M.F. Guest, W.R. Rodwell, Mol. Phys. **32**, 1075 (1976)
4. S.-K. Shih, S.D. Peyerimhoff, R.J. Buenker, Chem. Phys. **17**, 391 (1976)
5. Y. Hatano, Chem. Phys. Lett. **56**, 314 (1978)
6. A. Rauk, S. Collins, J. Mol. Spectr. **105**, 438 (1984)
7. G.H.F. Diercksen, P.W. Langoff, Chem. Phys. **112**, 227 (1987)
8. I. Cacelli, V. Carravetta, R. Moccia, Chem. Phys. **120**, 51 (1988)
9. V. Galasso, J. Phys. B **22**, 2241 (1989)
10. G. Theodorakopoulos, I.D. Petasalakis, Chem. Phys. Lett. **178**, 475 (1991)
11. B. Heumann, R. Düren, R. Schinke, Chem. Phys. Lett. **180**, 583 (1991)
12. R. Roberage, D. Salahub, J. Chem. Phys. **70**, 1177 (1979)
13. W.C. Price, J. Chem. Phys. **4**, 147 (1936)
14. K. Watanabe, A.S. Jursa, J. Chem. Phys. **41**, 1650 (1964)
15. F.W.E. Knoop, Ph.D. thesis, Leiden (1972)
16. H. Masuko, Y. Morioko, M. Nakamura, E. Ishiguro, M. Sasanuma, Can. J. Phys. **57**, 745 (1979)
17. M.N.R. Ashfold, W.S. Hartree, A.V. Salvata, B. Tutcher, A. Walker, J. Chem. Soc. Faraday Trans. **86**, 2027 (1990)
18. T. Abuain, I.C. Walker, D.F. Dance, J. Chem. Soc. Faraday Trans. **82**, 811 (1986)
19. E.A. Walters, N.C. Blais, J. Chem. Phys. **75**, 4208 (1981)
20. J.H.D. Eland, Int. J. Mass. Spectrom. Ion. Phys. **31**, 161 (1979)
21. R.L. Cook, F.C. DeLucia, P.J. Helminger, J. Mol. Struc. (Theochem) **28**, 237 (1975)
22. C.E. Brion, D.S.C. Lee, J. Electron Spectrosc. Relat. Phenom. **12**, 77 (1977)
23. F.A. Gianturco, D.G. Thompson, J. Phys. B **13**, 613 (1980)

24. A. Jain, D.G. Thompson, J. Phys. B **17**, 443 (1983)
25. F.A. Gianturco, J. Phys. B **24**, 4627 (1991)
26. B.H. Lengsfield, T.N. Rescigno, C.W. McCurdy, private communication (1992)
27. L.E. Machado, E.P. Leal, L. Mu-Tao, L.M. Brescansin, J. Mol. Struc. (Theochem) **335**, 37 (1995)
28. M.T. do N. Varella, M.H.F. Bettega, M.A.P. Lima, L.G. Ferreira, J. Chem. Phys. **111**, 6396 (1999)
29. A P.P. Natalense, M.T. do N. Varella, M.H.F. Bettega, L.G. Ferreira, M.A.P. Lima, Brazillian, J. Phys. **31**, 15 (2001)
30. K. Rohr, J. Phys. B **11**, 4109 (1978)
31. K. Rohr, private communication (1983)
32. V.F. Sokolov, Yu.A. Sokolova, Sov. Tech. Phys. Lett. **7**, 268 (1981)
33. C. Szymytkowski, K. Maciag, Chem. Phys. Lett. **129**, 321 (1986)
34. B.P. Marinkovic, Ph.D. thesis, University of Beograd (unpublished, 1985)
35. R.J. Gulley, M.J. Brunger, J. Buckman, J. Phys. B **26**, 2913 (1993)
36. K. Kraus, Z. Natursforsch. **16a**, 1378 (1961)
37. K. Jager, A. Henglein, Z. Natursforsch. **21a**, 1251 (1966)
38. F. Fiquet-Fayard, J.P. Ziesel, R. Azria, M. Tronc, J. Chiari, J. Chem. Phys. **56**, 254 (1972)
39. R. Azria, M. Tronc, S. Goursaud, J. Chem. Phys. **56**, 4234 (1972)
40. R. Azria, Y.Le. Coat, G. Lefevre, D. Simon, J. Phys. B **12**, 679 (1979)
41. L. Sanche, G.J. Schulz, J. Chem. Phys. **58**, 479 (1973)
42. L.A. Morgan, C.J. Gillan, J. Tennyson, X. Chen, J. Phys. B **30**, 4087 (1997)
43. L.A. Morgan, J. Tennyson, C.J. Gillan, Comput. Phys. Commun. **114**, 120 (1998)
44. S. Kaur, K.L. Baluja, J. Phys. B **38**, 3917 (2005)
45. M. Gupta, K.L. Baluja, J. Phys. B **38**, 4057 (2005)
46. M. Gupta, K.L. Baluja, Phys. Rev. A **73**, 042702 (2006)
47. N. Sanna, F.A. Gianturco, Comput. Phys. Commun. **114**, 142 (1998)
48. *Atomic and Molecular Processes: an R-matrix Approach*, edited by P.G. Burke, K.A. Berrington (Institute of Physics Publishing, Bristo, 1993)
49. C.J. Gillan, J. Tennyson, P.G. Burke, *Computational Methods for Electron-Molecule Collisions*, edited by W.M. Huo, F.A. Gianturco (Plenum, New York, 1995)
50. J. Tennyson, J. Phys. B **29**, 6185 (1996)
51. A. Faure, J.D. Gorfinkiel, L.A. Morgan, J. Tennyson, Comput. Phys. Commun. **144**, 224 (2002)
52. K.L. Baluja, P.G. Burke, L.A. Morgan, Comput. Phys. Commun. **27**, 299 (1982)
53. E. Magnusson, H.F. Schaefer III, J. Chem. Phys. **83**, 5721 (1985)
54. T.H. Dunning, P.J. Hay, *Methods of Electronic Structure Theory*, edited by H.F. Schaefer (Plenum, New York, 1977)
55. T.H. Edward, N.K. Moncur, L.E. Snyder, J. Chem. Phys. **46**, 2139 (1967)
56. A.J. Russell, M.A. Spackman, Molecular Phys. **90**, 251 (1997)
57. F.A. Gianturco, A. Jain, Phys. Rep. **143**, 347 (1986)
58. A. Jain, D.G. Thompson, Comput. Phys. Commun. **32**, 367 (1984)
59. J. Tennyson, C.J. Noble, Comput. Phys. Commun. **33**, 421 (1984)
60. S.I. Chu, A. Dalgarno, Phys. Rev. A **10**, 788 (1974)
61. G. Herzberg, *Molecular spectra and Molecular structure* (Krieger publishing company, Florida, 1996)